AIAA SciTech Forum
8-12 January 2024, Orlando, FL
AIAA SCITECH 2024 Forum

10.2514/6.2024-2561

Analysis of streaks in unstratified and stratified wakes

Sheel Nidhan *, Akhil Nekkanti †, Oliver T. Schmidt‡, and Sutanu Sarkar§
Department of Mechanical and Aerospace Engineering, University of California San Diego, CA 92093, USA

A turbulent circular disk wake [1] is investigated through visualizations, conditional averaging, and spectral analysis to analyze the presence of large-scale streaks. The near wake and intermediate wake are dominated by the vortex shedding mode residing at $m = 1, St = 0.135$ in the unstratified wake ($Fr = \infty$). Once the influence of the $m = 1$ mode is filtered, large-scale streaks become apparent in the flow. These streaks predominantly reside at $m = 2$, $St \to 0$. The effect of stratification on streaks is investigated through the analysis of two body-based Froude numbers $Fr = 2$ and 10. Streaks are present and the lift-up mechanism is active in the near wake of the $Fr = 10$ wake. However, as the $Fr = 10$ wake evolves downstream, the signature of these streaks get weaker. The $Fr = 2$ wake is significantly different from the other two cases from the very beginning. Large-scale streaks are significantly attenuated and the energy at $St \to 0$ is notably lower than the other two cases throughout the course of its evolution. Conditionally averaged streamwise vorticity fields reveal that streaks are generated through the lift-up mechanism. Higher stratification diminishes the strength of the streamwise vortices thereby diminishing the lift-up effect.

I. Introduction

Large-scale streaks are one of the most common types of coherent structures in wall-bounded flows. Originally identified by Kline et al. [2], these structures manifest as long streamwise regions of positive and negative streamwise velocity fluctuations and can account for up to 75% of Reynolds shear stress [3]. Jiménez and Pinelli [4] showed that the presence of a wall is not a necessary condition for the formation of these streaky structures. In fact, a few studies in the past [5, 6] have reported the presence of streak-like structures in mixing layers. In recent times, more attention has been paid to the dynamics of streaks in jets. Nogueira et al. [7] applied spectral proper orthogonal decomposition (SPOD) on a PIV dataset of a circular turbulent jet at a high Reynolds number and demonstrated the presence of large-scale streaky structures in the near field (until $x/D = 8$). They further demonstrated that these structures exhibit large time scales and are associated with a low frequency of $St \to 0$. The numerical counterpart of the previous study was performed by Pickering et al. [8]. In wall-bounded flows, it is well-established that the lift-up mechanism [9, 10] leads to the generation of streaks. In the lift-up mechanism, streamwise vortices induce wall-normal velocities, bringing high-speed fluid from the outer region (in wall-bounded flows) to the inner region (near the wall), and vice versa. The subsequent breaking of these streaks is an important component of the self-sustaining cycle of wall turbulence [11]. The presence of the lift-up mechanism has been reported in turbulent jets [7, 8, 12]. These counter-rotating vortices that cause lift-up are of particular importance in aviation where the lift force on the airplane wing produces a pair of counter-rotating trailing vortices. These vortices can persist for large downstream distance and can affect the flight of airplanes behind.

Motivated by these studies, we investigate a canonical bluff-body turbulent wake, namely the disk wake, to detect the presence (or absence) of large-scale streaks in the flow. In addition to flow visualizations and conditional averaging analysis, we utilize SPOD [13] to shed light on these structures. In the atmosphere, temperature and thereby density variability can affect the way vortices shed from an airplane evolve. Hence, we also extend our investigation to examine the influence of buoyancy effects on the formation and significance of large-scale streaks in the wake flow. Previous studies by Nidhan et al. [14] have shown that the dominance of the vortex shedding (VS) mode, in terms of its contribution to the total turbulent kinetic energy (TKE), increases with increasing buoyancy. Specifically, they found that the VS mode is more dominant at $Fr = 2$ compared to $Fr = 10$ and $Fr = \infty$. Additionally, research on the impact of stratification on channel flow conducted by García-Villalba and del Álamo [15] revealed that stratification has little effect on the near-wall streaks while damping the streaks in the outer region. In the unstratified wake, we observed a different behavior, where the dominance of streaks is concentrated in the $m = 2$ mode with a low frequency of $St \to 0$.

*S. N. and A.N. contributed equally
†Postdoctoral Scholar, Division of Engineering and Applied Science, California Institute of Technology, Pasadena, CA 91125, USA
‡Associate Professor, Department of Mechanical and Aerospace Engineering, Senior Member AIAA.
§Professor, Department of Mechanical and Aerospace Engineering, AIAA Associate Fellow

These streaks form as a result of the self-interaction of the VS mode [16]. Therefore, it is intriguing to explore whether this mechanism persists under increasingly stronger stratification conditions.

The rest of the paper is organized as follows. In section II we present a brief description of the dataset employed in this study. Section III gives a brief description of SPOD methodology. Results are presented in section IV and finally the paper is concluded in section VI.

II. Dataset description

The datasets employed in this study are obtained from large eddy simulations (LES) of flow past a circular disk at a body-based Reynolds number $Re = U_\infty D/\nu = 50,000$, presented in Chongsiripinyo and Sarkar [1]. Here, U_∞ represents the freestream velocity, D is the diameter of the disk, and ν is the kinematic viscosity. For the current work, the chosen cases involve three different body-based Froude numbers $Fr = U_\infty/ND = \infty, 10, 2$. Here, N is the buoyancy frequency given as $N = \sqrt{-(g/\rho_o)\mathrm{d}\rho_b/\mathrm{d}z}$, where density ρ is decomposed as $\rho = \rho_o + \rho_b(z) + \rho'(x, y, z, t)$.

The filtered Navier-Stokes equations, subject to the solenoidal velocity condition, were numerically solved on a structured cylindrical grid. The grid covers a radial distance of $r/D = 15$ and 80 for the unstratified and stratified cases, respectively. For the analysis presented in this draft, however, we will focus only until the radial extent of $r/D = 15$ for the stratified cases. All cases span a streamwise distance of $x/D = 125$. To represent the circular disk in the simulation domain, an immersed boundary method [17] is utilized, while the LES model employs the dynamic Smagorinsky model [18]. The grid comprises $N_r = 365$ points for the unstratified case and $N_r = 531$ points for stratified cases in the radial direction, $N_\theta = 256$ points in the azimuthal direction, and $N_x = 4096$ points in the streamwise direction. The simulation is performed at high resolution, with a streamwise grid resolution of $\Delta x = 10\eta$ at $x/D = 10$, where η denotes the Kolmogorov length scale. As the distance reaches $x/D = 125$, the resolution improves further to $\Delta x < 6\eta$, thereby reducing the reliance on the subgrid model. For a more comprehensive understanding of the numerical methodology and details on the grid quality, interested readers are referred to Chongsiripinyo and Sarkar [1].

III. Spectral Proper Orthogonal Decomposition

SPOD is the frequency-domain variant of proper orthogonal decomposition. It computes monochromatic modes that are optimal in terms of the energy norm of the flow, e.g., turbulent kinetic energy (TKE) for the wake flow at hand. The SPOD modes are the eigenvectors of the cross-spectral density matrix, which is estimated using Welch's approach [19] as

$$\frac{1}{n_{\mathrm{blk}}}\hat{\mathbf{Q}}_l\hat{\mathbf{Q}}_l^*\mathbf{W}\mathbf{\Phi}_l = \mathbf{\Phi}_l\mathbf{\Lambda}_l \tag{1}$$

where $\hat{\mathbf{Q}}_l$, $\mathbf{\Phi}_l$, $\mathbf{\Lambda}_l$, are the Fourier realizations, SPOD modes and SPOD eigenvalues at frequency index l, and $\mathbf{W}$ is a positive-definite Hermitian matrix that accounts for the component-wise and numerical quadrature weights.The matrices $\mathbf{\Lambda}_l = \mathrm{diag}(\lambda_l^{(1)}, \lambda_l^{(2)}, \cdots, \lambda_l^{(n_{\mathrm{blk}})})$, where by convention $\lambda_l^{(1)} \geq \lambda_l^{(2)} \geq \cdots \geq \lambda_l^{(n_{\mathrm{blk}})}$, and $\mathbf{\Phi}_l = [\boldsymbol{\phi}_l^{(1)}, \boldsymbol{\phi}_l^{(2)}, \cdots, \boldsymbol{\phi}_l^{(n_{\mathrm{blk}})}]$ contain the SPOD energies and modes, respectively. Readers are referred to Towne et al. [13], and Schmidt and Colonius [20] for detailed mathematical derivation and algorithmic implementation. Here, we perform SPOD on various 2D streamwise planes ranging from $x/D = 10$ to 100, at a spacing of $5D$. The spectral estimation parameters used here are $n_{\mathrm{fft}} = 512$ and $n_{\mathrm{ovlp}} = 256$, resulting in $n_{\mathrm{blk}} = 27$ SPOD modes for each St.

A. Reconstruction using convolution approach

The convolution strategy proposed by [21] is employed for low-dimensional reconstruction of the flow field. This involves computing the expansion coefficients by convolving the SPOD modes over the data one snapshot at a time,

$$\mathbf{a}_l^{(i)}(t) = \int_{\Delta T}\int_{\Omega}\left(\phi_l^{(i)}(x)\right)^*\mathbf{W}(x)\mathbf{q}(x, t+\tau)w(\tau)e^{-i2\pi f_l\tau}\mathrm{d}x\mathrm{d}\tau. \tag{2}$$

Here, $w(\tau)$ is the Hamming windowing function and Ω is the spatial domain of interest. The data at time t is then reconstructed as

$$\mathbf{q}(t) \approx \sum_l\sum_i a_l^{(i)}(t)\boldsymbol{\phi}_l^{(i)}e^{-i2\pi f_l t}. \tag{3}$$

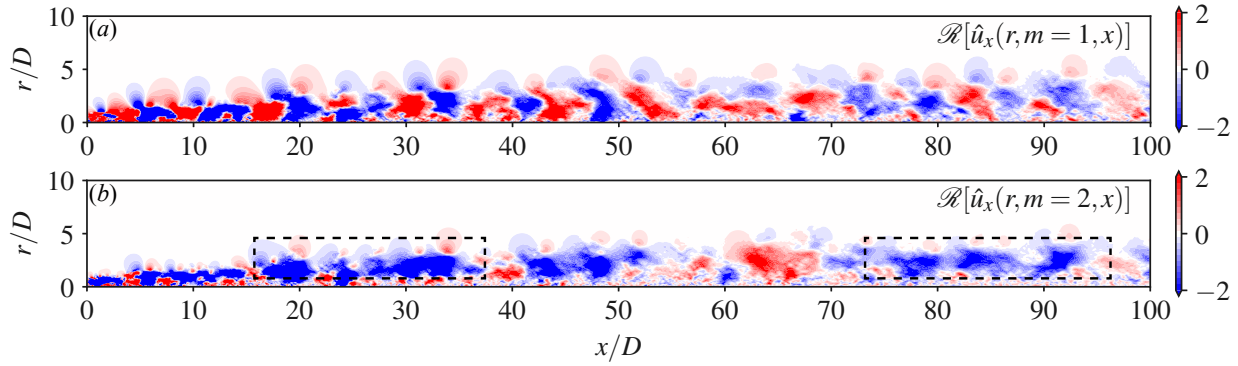

Fig. 1 Azimuthally decomposed instantaneous fields of the streamwise velocity (u'_x) fluctuations for azimuthal modes (a) $m = 1$ and (b) $m = 2$, for the unstratified wake ($Fr = \infty$). Rectangular boxes in (b) show large-scale streaks in the $m = 2$ field.

IV. Unstratified wakes

Figure 1 shows an instantaneous flow snapshot in the wake region for the unstratified wake, in particular the azimuthal modes $m = 1$ and $m = 2$. The snapshot covers a downstream distance of $0 < x/D < 100$, obtained through a Fourier transform in the azimuthal direction θ. In the $m = 1$ mode (figure 1a), the presence of a wavelength $\lambda/D = 1/St_{VS}$ is evident throughout the domain. Here, St_{VS} represents the vortex shedding frequency, estimated to be approximately 0.13-0.14. This observation aligns with prior studies [22–24] that also confirm the existence of the vortex shedding mode at significantly larger downstream locations, around $O(100D)$ from the disk. In contrast, the $m = 2$ mode (figure 1b) exhibits distinct elongated structures throughout the domain. Notably, the structures within the dashed rectangular boxes are of interest. These structures can extend up to a streamwise extent of $\lambda_x/D \approx 25$ (specifically within the range $70 < x/D < 95$), significantly surpassing the wavelength of the vortex shedding mode, approximately $\lambda_x/D \approx 7$.

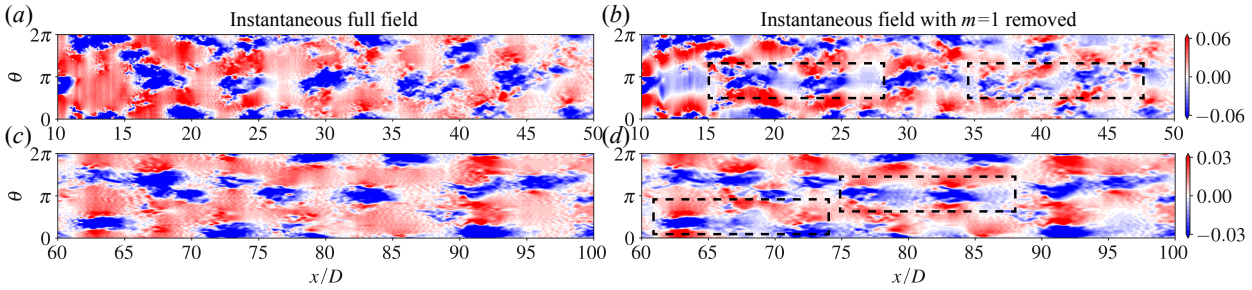

Fig. 2 Instantaneous streamwise velocity on $x/D - \theta$ planes for the unstratified ($Fr = \infty$) wake at $r/D = 1.25$ (a,b) and $r/D = 2.5$ (c,d). (a,c) show the full streamwise velocity field and (b,d) show the field with $m = 1$ contribution removed. Rectangular boxes in (b, d) emphasize the large-scale streaks in the flow field.

Figure 2 (a, c) provides a visual representation of the instantaneous streamwise velocity field in the near-intermediate and intermediate-far wake regions of the unstratified case. These fields are shown on an $x/D - \theta$ plane, which is constructed by unrolling the cylindrical surface at a constant r/D. Specifically, the near-intermediate field (figure 2a) corresponds to $r/D = 1.25$, while the intermediate-far field (figure 2c) corresponds to $r/D = 2.5$. Both figures exhibit clear vortex shedding structures, with an approximate wavelength of $\lambda_x/D \approx 7$. By filtering out the contribution of the vortex shedding mode at $m = 1$ azimuthal wavenumber [22–24], the presence of streaks in the unstratified wake becomes more prominent, as depicted in figure 2(b, d). Notably, the structures enclosed within the dashed rectangular boxes in figure 2(b, d) attract attention. These observations, combined with the findings from figure 1 and the existing literature on turbulent jets [7, 8], serve as strong evidence for the existence of large-scale streaks in turbulent wakes.

Next, we compare the dynamics of the streaky structure ($m = 2, St \to 0$) and the vortex shedding structure ($m = 1, St = 0.135$) in physical space. For this purpose, the flow field is reconstructed using the leading five SPOD modes of these two structures. The azimuthal wavenumber $m = 2$ is chosen because it is energetically dominant at

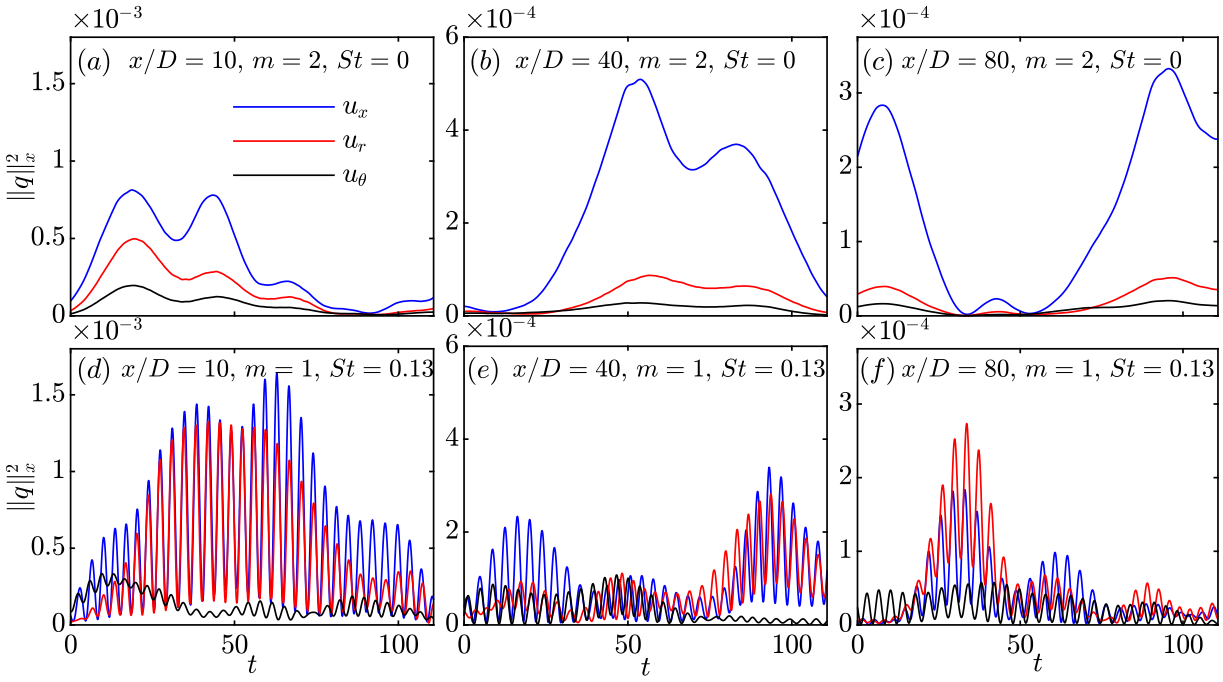

Fig. 3 Component-wise instantaneous energy reconstructed from the $m = 2$ streaky structures in the top row (a-c) and vortex shedding structures (d-f) in the bottom row. The plane integral of the energy is shown at various streamwise locations: (a, d) $x/D = 10$, (b, e) $x/D = 40$ and (c, f) $x/D = 80$. Flow reconstruction uses the leading five SPOD modes. The oscillation frequency of the reconstructed energy in (d-f) is twice that of the VS frequency.

$St \to 0$ [16, 23]. The reconstruction is performed using the convolution strategy described in section §III.A. The instantaneous energy of the three fluctuation components, u'_x, u'_r, and u'_θ at $x/D = 10$, 40, and 80, within the time interval $t \in [0, 110]$, is shown in figure 3. This time interval corresponds to the first five blocks used for SPOD, and is representative of the entire reconstructed flow fields. The difference between the time scale of the streaks and vortex-shedding modes is apparent, with the former exhibiting a much longer time scale than the latter. For the streaky structures, the energy of u'_x is significantly higher than that of u'_r and u'_θ. In contrast, u'_x and u'_r components have comparable energy for the vortex shedding modes. The dominance of the streamwise component over its radial and azimuthal counterparts is one salient feature of streaks. The finding of u'_x dominance is in agreement with those of Boronin et al. [25, see figure 11] and Pickering et al. [8, see figure 10] in the context of round jets, indicating similarity in streak formation between jets and wakes. The lift-up mechanism, in which the streamwise vortices lift up and push down the low-speed and high-speed fluid, respectively, is responsible for elongated streaks accompanied by an amplification of u'_x.

V. Stratified Wakes

Now that the presence of streaks in unstratified wakes has been identified, we shift our focus to stratified wakes. Two stratified cases are considered: $Fr = 10$ and 2, which correspond to a weakly stratified case and a more strongly stratified case, respectively.

Figure 4 presents the mean streamwise velocity contours (top row) and TKE contours (bottom row) for all three stratification levels at $x/D = 40$. Both the statistical quantities remain axisymmetric for the unstratified wake (leftmost column). For the weakly stratified case of $Fr = 10$, one can notice a moderate deviation from the axisymmetry at $x/D = 40$. Finally, for the strongest stratification case $Fr = 2$, the contours are squished in the vertical direction as a consequence of the strong hindrance imposed by gravity to the motion in the vertical direction. Figure 4 shows that by $x/D = 40$, an appreciable effect of stratification can be observed in both $Fr = 2$ and $Fr = 10$ wakes. In what follows, we will further investigate how stratification influences the streaky structures in the turbulent wake.

In figure 5, we employ Taylor's hypothesis at $x/D = 10$ for all three cases. At this location, we convert time

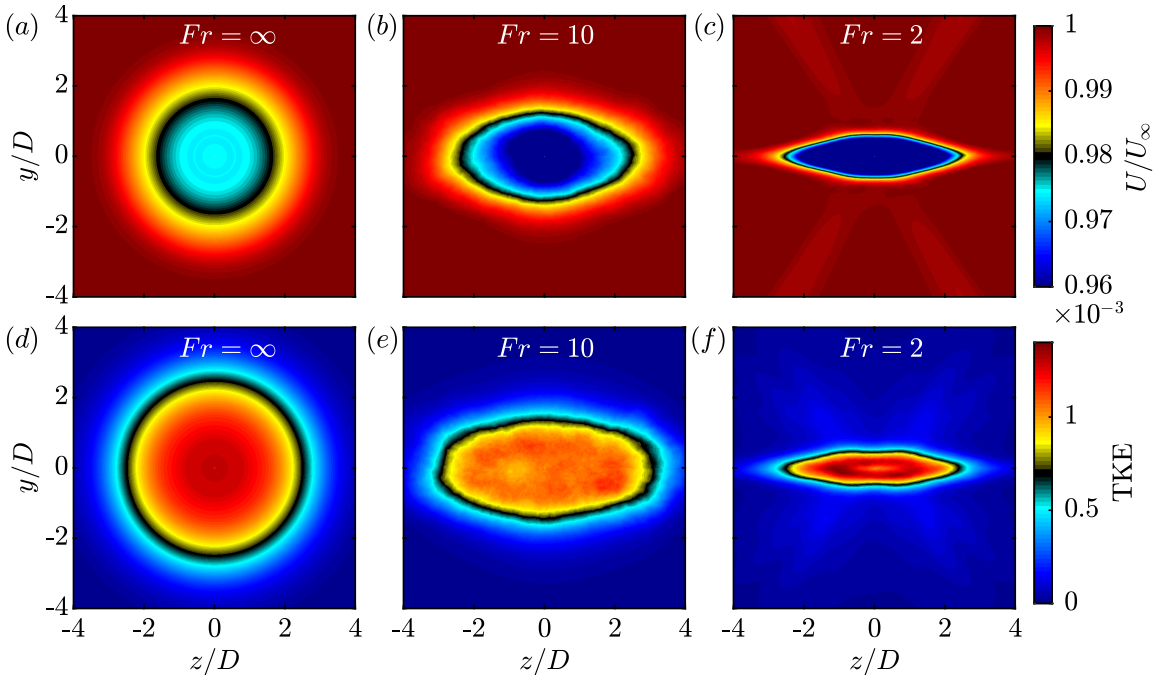

Fig. 4 Mean (*a*,*b*,*c*) and TKE (*d*,*e*,*f*) contours at the streamwise location $x/D = 40$ for different levels of stratification: (a, d) $Fr = \infty$; (b, e) $Fr = 10$; (c, f) $Fr = 2$.

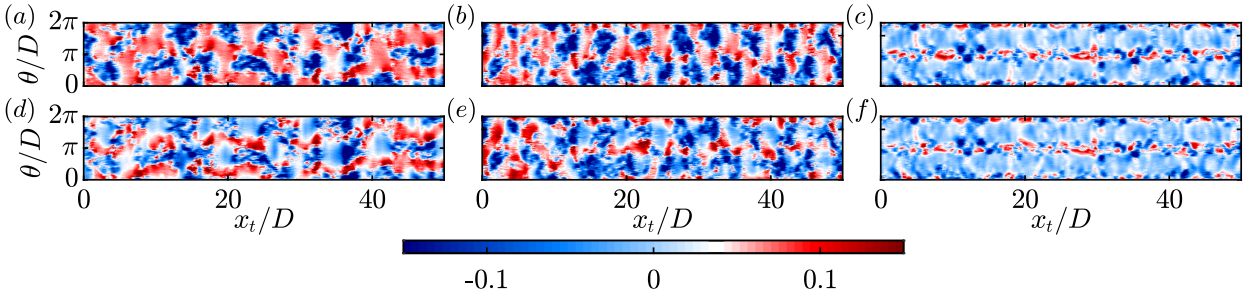

Fig. 5 Streamwise velocity fluctuations u'_x on $x_t/D - \theta$ plane for $Fr = \infty$ (a, d), $Fr = 10$ (b, e), and $Fr = 2$ (c, f) wakes. $x/D = 10$ and $r/D = 0.8$ is used across all three cases. Top row includes all frequency components while the the vortex shedding frequency is removed *a priori* in the bottom row.

t to a pseudo-streamwise distance $x_t \approx U_\infty t$. Here, we assume that the convective speed of the structures can be well-approximated by the freestream velocity U_∞ since the defect velocity $U_d << U_\infty$ at these locations. In Nekkanti et al. [16], we further quantified that U_d drops below $\sim 12\%$ by $x/D = 10$ and only continues to drop further as the wake develops downstream.

For the unstratified wake (figure 5a, d), once the vortex shedding frequency is filtered out at $x/D = 10$, the large-scale streaks become readily apparent in figure 5(d). Likewise, in the $Fr = 10$ wake as well (middle column), the removal of vortex shedding bring out the presence of large-scale streaks in the near wake region. However, the $Fr = 2$ case is qualitatively different than the other two cases. Firstly, there is significantly less activity for $\theta \in (0, \pi)$ and $\theta \in (\pi, 2\pi)$ as compared to locations clustered near $\theta = 0$ and $\theta = \pi$. This is indicative of the fact that stratification restricts the vertical motions as early as $x/D = 10$ in the $Fr = 2$ wake and most of the turbulent activity is confined close to the horizontal plane $z = 0$. Secondly, in the horizontal plane $z = 0$ (in Cartesian coordinates) or $\theta = 0$ and π (in cylindrical coordinates), large-scale streaks similar to the $Fr = \infty$ or 10 wakes can not be discerned.

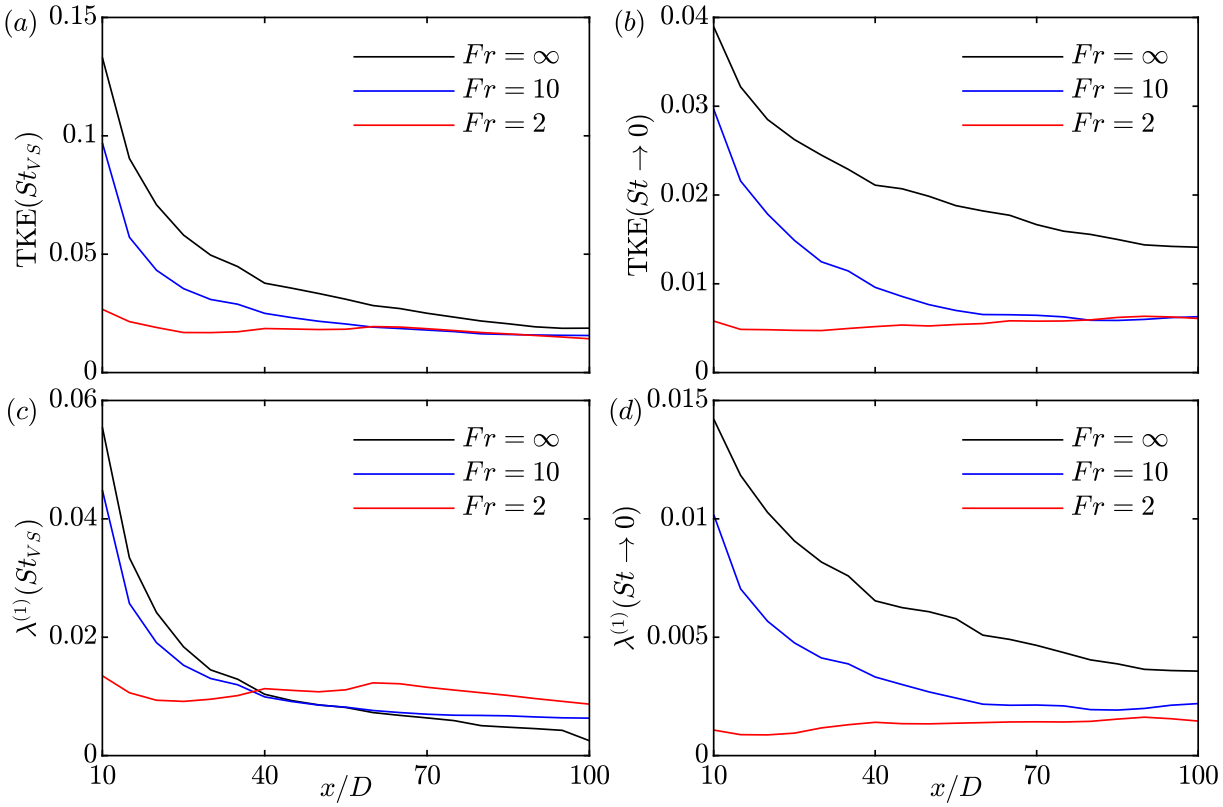

Fig. 6 TKE (a, b) and leading SPOD eigenvalue (c,d) of the vortex shedding structures (a,c) and streaky structures (b,d) for different Froude numbers.

Next, we investigate the effect of stratification on the energy of the vortex shedding and streaky structures. To achieve this, we perform SPOD on 2D planes at different streamwise locations. The TKE of vortex shedding modes and streaks is computed as $\mathrm{TKE}(St_{VS}) = \sum_i \lambda^{(i)}(St = 0.135)$, and $\mathrm{TKE}(St \to 0) = \sum_i \lambda^{(i)}(St \to 0)$, respectively. Figure 6(a, b) illustrates the TKE at these frequencies and three Froude numbers. It is observed that higher stratification leads to a diminished energy of vortex shedding and streaky structures. This effect is particularly noticeable in the near wake. In the far wake, beyond $x/D > 60$, the TKE contained in these structures for $Fr = 10$ and 2 becomes comparable. In comparison to their unstratified counterparts, stratified wakes demonstrate a reduction in TKE due to the suppression of vertical motions by stratification.

Figure 6 (c), and (d) show the leading SPOD eigenvalue at the vortex-shedding, and zeroth frequency, respectively. A similar trend is observed in the near wake, with higher stratification containing lower energy. However, a notable difference is observed at the vortex shedding frequency, where the first SPOD eigenvalue at $Fr = 2$ surpasses the values for the other two cases beyond $x = 40$. For $x \geq 40$, only the $Fr = 2$ wake resides in the strongly stratified turbulence (SST) regime [1]. In this regime, horizontal shear re-energizes the vortex shedding structures. In contrast, streaky structures are less affected by horizontal shear. Streaks are generated through the lift-up mechanism, where $\partial u_x/\partial t \propto -u_z \partial U(z)/\partial z$ for inviscid flow [9]. Consequently, streaks are more sensitive to vertical shear. Furthermore, since u_z in the wake is suppressed by stabilizing buoyancy, the first SPOD eigenvalue at $St \to 0$ is lower for lower Fr.

A. Lift-up mechanism in the unstratified and stratified wakes

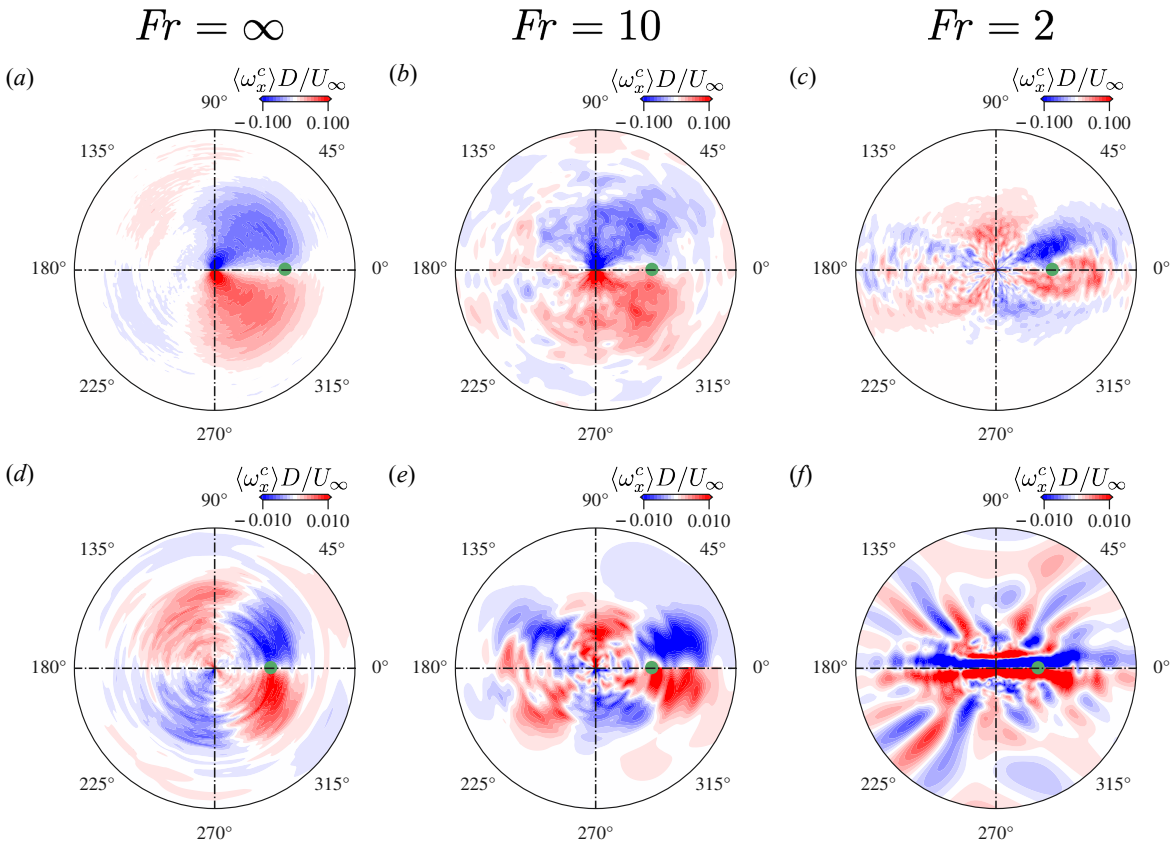

Fig. 7 Conditionally-averaged streamwise vorticity field $\langle\omega_x^c\rangle$ at $x/D = 10$ (top row) and $x/D = 40$ (bottom row) for different Fr. The green dot shows the location of the conditioning point: (a, b, c) $r/D = 0.8, \theta = 0°$, (d, e) $r/D = 2, \theta = 0°$, (f) $r/D = 1.5, \theta = 0°$. The radial domain extends until $r/D = 2$ at $x/D = 10$ and until $r/D = 5$ at $x/D = 40$.

Streamwise streaks are commonly observed in turbulent free shear flows and wall-bounded flows, and their formation is often associated with the lift-up mechanism [9, 10]. The lift-up mechanism involves the sweeping of fluid from regions of high-speed to low-speed and vice versa, leading to the formation of high-speed and low-speed streaks. The crucial role of the lift-up mechanism in various fundamental phenomena, such as subcritical transition in shear flows, self-sustaining cycle in wall-bounded flows, and disturbance growth in complex flows, has been extensively reviewed by Brandt [26].

To investigate the presence of the lift-up mechanism in the wake, we examine conditional averages of streamwise vorticity fluctuations (ω_x) at two representative locations in all three cases: $x/D = 10$ (top row) and $x/D = 40$ (bottom row) in figure 7. The conditional average, $\langle \omega_x^c \rangle$, is designed to extract the structure of streamwise vorticity on a constant-x plane during times of large streamwise velocity fluctuations. The condition is based on the criterion that $u'_x \geq c(u'_x)^{\text{rms}}$ at a specified point P (green point) on the plane, and $\langle \omega_x^c \rangle$ represents the temporal average of all $\omega_x(t)$ that satisfy this condition. The terms $(u'_x)^{\text{rms}}$ represents the root mean square (r.m.s.) values of streamwise velocity fluctuations at the conditioning points. The choice of $c \in (0, 1]$ exhibits moderate sensitivity. Therefore, a compromise value of $c = 0.5$ is used to balance the identification of intense events with the retention of sufficient snapshots for conditional averaging. The conditional point P is chosen to lie at $\theta = 0°$. For the unstratified wake, to increase the ensemble size for the conditional average, we exploit the rotational invariance of statistics by applying the condition to a new point P_1 at the same r/D but a different value of θ. The resulting $\langle \omega_x^c \rangle$ field is then rotated to align with point P. This approach effectively expands the ensemble used for the conditional average. This methodology can not be applied for the $Fr = 10$ and 2 wakes since the azimuthal symmetry is destroyed by the stratification.

For the unstratified wake (figure 7*a*, *d*), two opposite-signed coherent vortices are visible in the conditionally averaged field, pulling the high-speed fluid from the outer wake to the inner wake, creating the so-called lift-up effect. As we move further downstream to $x/D = 40$ (figure 7*d*), the organization of the vortices becomes more complex. However, around the conditioning point, still two rolls of oppositely-signed streamwise vorticity are present. For the wake characterized by $Fr = 10$, the organization of the mean cross-stream vorticity ($\langle \omega_x^c \rangle$) at the downstream location of $x/D = 10$ closely resembles that of the unstratified wake. However, a slight increase in noise is observed, attributed to the limited ensemble size in the stratified wake, in contrast to the unstratified case where enhanced ensemble size was present, benefiting from rotational invariance. However, the spatial organization of $\langle \omega_x^c \rangle$ at $x/D = 40$ is very different in the $Fr = 10$ wake. At $x/D = 40$, the vortices are 'squished' in the vertical direction due to buoyancy and the size of these vortex rolls are smaller. This change in the organization and structure of the vortex rolls is further intensified for $Fr = 2$ (figure 7*c*, *f*). At $x/D = 10$, the conditionally averaged vortex field is significantly less intense for $Fr = 2$ as compared to $Fr = 10$ or $Fr = \infty$. The reduced intensity suggests that the lift-up effect is attenuated at higher stratification. At $x/D = 40$, significant streamwise vorticity is present in the internal waves away from the wake core. Furthermore, while the opposite-signed vortices are present around the conditioning point, they appear as horizontally layered structures rather than rolls.

VI. Conclusions

In this study, we investigate the turbulent wake of a circular disk at a Reynolds number of $Re = 50,000$ with three levels of stratification: $Fr = \infty$, 10, and 2. By filtering out the $m = 1$ azimuthal wavenumber, another coherent structure, namely streaks, becomes apparent. These streaks exhibit significantly larger wavelengths and timescales compared to the vortex shedding structures. The dynamical significance of streaks increases progressively from the near wake to the far wake. They are associated with a frequency of $St \to 0$, and the azimuthal wavenumber $m = 2$ contributes most to their energy. Similar to other turbulent flows such as boundary layers, channel flows, and jets, streaks are generated through the lift-up mechanism in wakes. The lift-up mechanism consists of two counter-rotating streamwise vortices that lift up and push down the low-speed and high-speed fluid, resulting in elongated streaks with large streamwise velocity.

In stratified flows, the lift-up effect and resulting streaks are diminished. In the weakly stratified case with $Fr = 10$, streaky structures are observable in the near wake, with their energy decreasing downstream. The impact of stratification becomes more pronounced in the highly stratified case with $Fr = 2$, where only traces of streaky structures are observed in the near and far wakes. Larger stratification confines the streaks to the horizontal plane, suppressing vertical motion. The suppression of vertical motion is more prominent in higher stratification, leading to a reduction in the energy of the streaky structures. Conditionally averaged fields demonstrate a decrease in the intensity of streamwise vortices in stratified wakes. The buoyancy in the vertical direction compresses the vortices, resulting in a reduction in the size of the vortex rolls. These findings clearly indicate that stratification attenuates the lift-up effect, thereby diminishing the presence of streaks.

This study underscores the need for a more detailed examination of the impact of stratification on streaks. Future work could benefit from an energy budget analysis, specifically examining how buoyancy affects vertical and horizontal production. Recent work by [16] delved into the nonlinear interactions of vortex shedding modes on streaky structures. Exploring how stratification influences these nonlinear interactions could be a worthwhile endeavor.

Acknowledgments

We acknowledge the support of Office of Naval Research (ONR) grant N00014-20-1-2253.

References

[1] Chongsiripinyo, K., and Sarkar, S., "Decay of turbulent wakes behind a disk in homogeneous and stratified fluids," *J. Fluid Mech.*, Vol. 885, 2020, p. A31.

[2] Kline, S. J., Reynolds, W. C., Schraub, F. A., and Runstadler, P. W., "The structure of turbulent boundary layers," *J. Fluid Mech.*, Vol. 30, No. 4, 1967, pp. 741–773.

[3] Lu, S. S., and Willmarth, W. W., "Measurements of the structure of the Reynolds stress in a turbulent boundary layer," *J. Fluid Mech.s*, Vol. 60, No. 3, 1973, pp. 481–511.

[4] Jiménez, J., and Pinelli, A., "The autonomous cycle of near-wall turbulence," *J. Fluid Mech.*, Vol. 389, 1999, pp. 335–359.

[5] Brown, G. L., and Roshko, A., "On density effects and large structure in turbulent mixing layers," *J. Fluid Mech.*, Vol. 64, No. 4, 1974, pp. 775–816.

[6] Liepmann, D., and Gharib, M., "The role of streamwise vorticity in the near-field entrainment of round jets," *J. Fluid Mech.*, Vol. 245, No. -1, 1992, p. 643.

[7] Nogueira, P. A. S., Cavalieri, A. V. G., Jordan, P., and Jaunet, V., "Large-scale streaky structures in turbulent jets," *J. Fluid Mech.*, Vol. 873, 2019, pp. 211–237.

[8] Pickering, E., Rigas, G., Nogueira, P. A. S., Cavalieri, A. V. G., Schmidt, O. T., and Colonius, T., "Lift-up, Kelvin–Helmholtz and Orr mechanisms in turbulent jets," *J. Fluid Mech.*, Vol. 896, 2020, p. A2.

[9] Ellingsen, T., and Palm, E., "Stability of linear flow," *Phys. Fluids*, Vol. 18, No. 4, 1975, p. 487.

[10] Landahl, M. T., "Wave breakdown and turbulence," *SIAM J. Appl. Math.*, Vol. 28, No. 4, 1975, pp. 735–756.

[11] Hamilton, J. M., Kim, J., and Waleffe, F., "Regeneration mechanisms of near-wall turbulence structures," *J. Fluid Mech.*, Vol. 287, 1995, pp. 317–348.

[12] Lasagna, D., Buxton, O. R. H., and Fiscaletti, D., "Near-field coherent structures in circular and fractal orifice jets," *Phys. Rev. Fluids*, Vol. 6, No. 4, 2021, p. 044612.

[13] Towne, A., Schmidt, O. T., and Colonius, T., "Spectral proper orthogonal decomposition and its relationship to dynamic mode decomposition and resolvent analysis," *J. Fluid Mech.*, Vol. 847, 2018, pp. 821–867.

[14] Nidhan, S., Schmidt, O. T., and Sarkar, S., "Analysis of coherence in turbulent stratified wakes using spectral proper orthogonal decomposition," *J. Fluid Mech.*, Vol. 934, 2022, p. A12.

[15] Garcia-Villalba, M., and Del Alamo, J. C., "Turbulence modification by stable stratification in channel flow," *Phys. Fluids*, Vol. 23, No. 4, 2011, p. 045104.

[16] Nekkanti, A., Nidhan, S., Schmidt, O. T., and Sarkar, S., "Large-scale streaks in a turbulent bluff body wake," *Journal of Fluid Mechanics*, Vol. 974, 2023, p. A47.

[17] Balaras, E., "Modeling complex boundaries using an external force field on fixed Cartesian grids in large-eddy simulations," *Comput. Fluids*, Vol. 33, No. 3, 2004, pp. 375–404.

[18] Germano, M., Piomelli, U., Moin, P., and Cabot, W. H., "A dynamic subgrid-scale eddy viscosity model," *Phys. Fluids*, Vol. 3, No. 7, 1991, pp. 1760–1765.

[19] Welch, P., "The use of fast Fourier transform for the estimation of power spectra: a method based on time averaging over short, modified periodograms," *IEEE Transactions on Audio and Electroacoustics*, Vol. 15, No. 2, 1967, pp. 70–73.

[20] Schmidt, O. T., and Colonius, T., "Guide to spectral proper orthogonal decomposition," *AIAA Journal*, Vol. 58, No. 3, 2020, pp. 1023–1033.

[21] Nekkanti, A., and Schmidt, O. T., "Frequency–time analysis, low-rank reconstruction and denoising of turbulent flows using SPOD," *J. Fluid Mech.*, Vol. 926, 2021, p. A26.

[22] Johansson, P. B. V., George, W. K., and Woodward, S. H., "Proper orthogonal decomposition of an axisymmetric turbulent wake behind a disk," *Phys. Fluids*, Vol. 14, No. 7, 2002, p. 2508.

[23] Johansson, P. B. V., and George, W. K., "The far downstream evolution of the high-Reynolds-number axisymmetric wake behind a disk. Part 2. Slice proper orthogonal decomposition," *J. Fluid Mech.*, Vol. 555, 2006, p. 387.

[24] Nidhan, S., Chongsiripinyo, K., Schmidt, O. T., and Sarkar, S., "Spectral proper orthogonal decomposition analysis of the turbulent wake of a disk at Re= 50 000," *Phys. Rev. Fluids*, Vol. 5, No. 12, 2020, p. 124606.

[25] Boronin, S., Healey, J., and Sazhin, S., "Non-modal stability of round viscous jets," *J. Fluid Mech.*, Vol. 716, 2013, pp. 96–119.

[26] Brandt, L., "The lift-up effect: the linear mechanism behind transition and turbulence in shear flows," *Eur. J. Mech. B*, Vol. 47, 2014, pp. 80–96.